JOURNAL OF MATERIALS SCIENCE 30 (1995) 1535–1538

Lifetime predictions of a glass-ceramic with machined flaws

T. GENT, D. TUCKER
NASA – Marshall Space Flight Center, Huntsville, AL 35812, USA

A dynamic fatigue study was performed on a Li_2O–Al_2O_3–SiO_2 glass ceramic to assess its susceptibility to delayed failure and to compare the results with those from a previous study. Fracture mechanics techniques were used to analyse the results for the purpose of making lifetime predictions. The material strength and lifetime was seen to increase due to the removal of residual stress through grinding and polishing. Influence on time-to-failure is addressed for the case with and without residual stress present.

1. Introduction

The glass-ceramic (Zerodur, Schott Glaswerke, Mainz, Germany) used in this study has been selected by NASA for the cylindrical mirror elements on the Advanced X-ray Astrophysics Facility. It contains 70%–78% by weight crystalline phase of high quartz, with a mean crystal size of 50–55 nm. The material maintains a near zero thermal expansion coefficient due to the positive thermal expansion of the vitreous phase and the negative thermal expansion of the crystalline phase [1]. This property makes it an excellent candidate for optical applications subject to thermal cycling.

This material was the subject of an earlier study to determine the susceptibility to delayed failure [2]. This previous study was based on the 230/270 grit surface given by the manufacturer. The grinding and polishing process reduces the surface flaw size and subsurface damage, and relieves residual stress by removing the material with successively smaller grinding media. This results in an increase in the strength of the optic during the grinding and polishing sequence. Thus, a second study was undertaken using samples with a surface finish identical to that which will be on the outer diameter of the mirror elements, to observe the effects of surface finishing on the time-to-failure predictions. The surface finish of the outer diameter was chosen for testing rather than the inner surface because the inner surface will undergo a more controlled grind and polish sequence. Thus the outer diameter will be the limiting factor in the strength of the optic.

An allowable stress can be calculated for this material based on modulus of rupture data; however, this does not take into account the problem of delayed failure. It is well known that many ceramic materials undergo delayed failure, due to stress corrosion, which can significantly shorten the lifetime of the article [3–10]. Fortunately, a theory based on fracture mechanics has been developed enabling lifetime predictions to be made for brittle materials susceptible to delayed failure [3–5]. Knowledge of the factors governing the rate of subcritical flaw growth in a given environment enables the development of relations between lifetime, applied stress, and failure probability for the material under study. Dynamic fatigue is one method of obtaining the necessary information to develop these relationships. In this study, the dynamic fatigue method was used to construct time to failure diagrams for 230/270 ground and polished Li_2O–Al_2O_3–SiO_2 glass-ceramic. The diagram was constructed using the following expression

$$\ln t_f = \ln B + \frac{(N-2)}{m_i}\ln\ln\left[\frac{1}{(1-F)}\right] + m_i \ln S_{oi} - N \ln S_a \quad (1)$$

where m_i and S_{oi} are the inert Weibull modulus and scaling parameter, respectively, F is the probability of failure, S_a is the applied stress, and B and N are fatigue constants.

Polishing material alleviates the residual stress and reduces the critical flaw size, increasing the strength of the material. Numerous investigations have addressed the effect of residual stress on strength and dynamic fatigue of glass through indentation fracture theory [11,12]. However, no criteria has been established to apply indentation fracture theory to machined flaws [13]. Consequently, one can only base analysis on the surface characteristics of the actual part.

2. Experimental procedure

Samples were delivered to NASA with a 600 grit surface finish and were then polished to meet the test criteria. The samples were 66 mm diameter and ground and polished to approximately 6 ± 0.2 mm. The polishing process was a control and grind polish, removing material equal to the diameter of the previous grit size. The grinding process used media of 30, 20, 12, and 5 μm with final polish utilizing a urethane pad and cerium oxide polishing compound.

Samples were tested in lots of 25 at stressing rates of 0.1, 6, 200, and 10000 MPa s^{-1} using a concentric ring

0022–2461

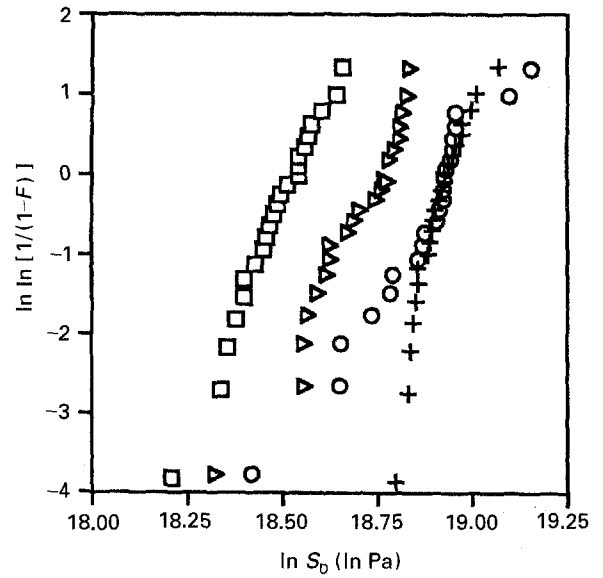

Figure 1 Strength distributions for dynamic fatigue of polished Li_2O–Al_2O_3–SiO_2 glass-ceramic. (●) 0.1 MPa s^{-1}, (▽) 6.0 MPa s^{-1}, (+) 200 MPa s^{-1}, (○) 10^4 MPa s^{-1}.

test fixture on a servo-hydraulic testing machine. The first three stressing rates were tested at room temperature in ambient air. The samples tested at 10000 MPa s^{-1} for inert strength were first dried in an oven at 110 °C for 24 h and placed in a desiccator until the test was performed. An environmental chamber was fabricated to enable the inert testing of these samples. The chamber was thoroughly purged with dry nitrogen and the samples exposed to this environment for 1 min prior to testing. The inert stressing rate, σ, can be verified using Equation 2 derived elsewhere [14]

$$\sigma = \frac{S_i^3}{B(N+1)} \tag{2}$$

Using B and N determined from the polished samples, the inert stressing rate was determined to be 166 MPa s^{-1}. Polished samples tested at 10^5 MPa s^{-1} were not significantly different from samples tested at 200 MPa s^{-1}, as seen in Fig. 1. The inert stressing rate for 230/270 was calculated to be 2.33×10^4 MPa s^{-1} using B and N determined in the previous study. The inert stressing rates used in both studies meet or exceed the values determined from Eq. 2.

Failure analysis was performed on each sample to determine the origin of failure, using a stereomicroscope at 128× or less.

3. Results and discussion

The breaking strength of each sample was calculated from the following equation

$$S_b = 1.08\frac{P_b}{t^2} \tag{3}$$

where S_b is the breaking stress or modulus of rupture, P_b is the breaking load, and t is the sample thickness. The constant 1.08 takes into account the sample and fixture geometry and Poisson's ratio [15]. The

TABLE I Results of dynamic fatigue concentric ring bend specimens

σ(MPa s^{-1})	m	lnS_0	R^2
0.1	11.84	18.53	0.99
6.0	9.61	18.76	0.95
200	18.28	18.94	0.89
1.0×10^4	7.74	18.95	0.94

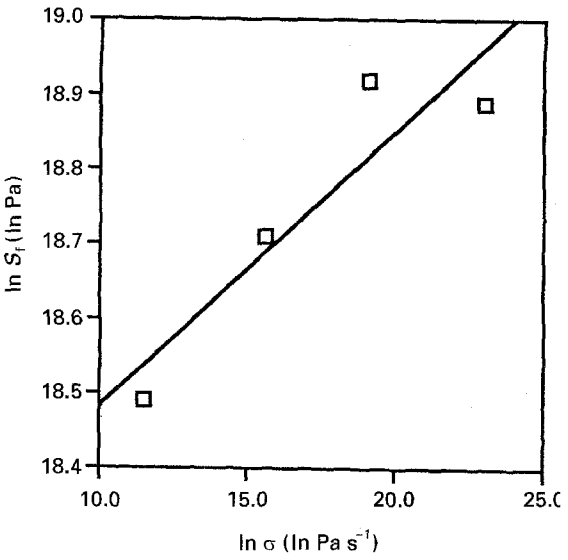

Figure 2 Dynamic fatigue data and insert strength data: median strength as a function of stress rate.

strength data are shown in Fig. 1, where S_b are plotted as a function of the failure probability, F, at each stressing rate. Failure probability was calculated from

$$F = \frac{(n - 0.5)}{N} \tag{4}$$

where n is the rank of the breaking stress of each sample and N is the total number of samples in the distribution. Each set of strength values was fitted to a two-parameter Weibull distribution by linear least-squares regression analysis of lnS_b on ln ln $[1/(1-F)]$ [14]. Estimates of the Weibull modulus and the scaling factor were obtained for the regression analysis and are shown with the strength data in Table I. Because the correlation coefficients were greater than 0.85, the two-parameter Weibull distribution was concluded to be acceptable and was used in the dynamic fatigue analysis.

The distributions in Fig. 1 exhibit deviations from linearity which could indicate a bimodal flaw distribution. However, failure analysis revealed that all specimens failed within the region of highest stress (i.e. within the area bounded by the load ring on the tensile surface). The error in tolerances of sample flatness and fixture design could cause the bimodal occurrence. It can also be seen in Fig. 1 that the distributions of the two highest stressing rates overlap somewhat. Recall that the calculated inert stressing rate for the polished surface was 168 MPa s^{-1}, the data confirm that increasing the stressing rate beyond the calculated value does not significantly change the strength distribution.

Median fracture stresses, S_f, used in the analysis of the dynamic fatigue results, are plotted in Fig. 2 as

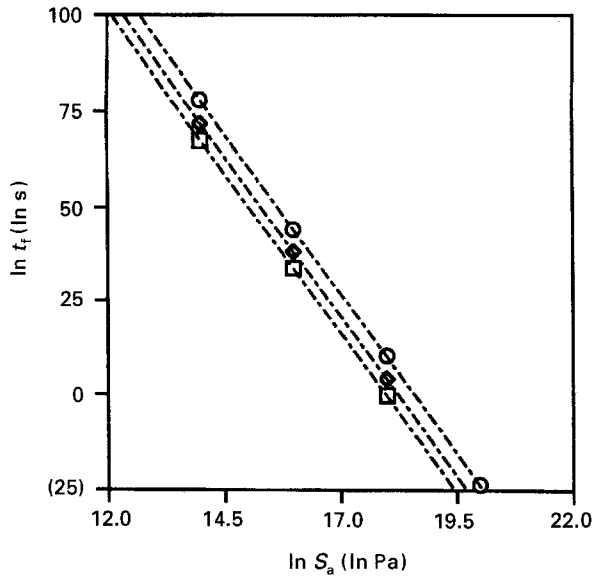

Figure 3 Time-to-failure diagram for polished Li_2O–Al_2O_3–SiO_2 glass-ceramic from dynamic fatigue data for F = (□) 0.001, (◇) 0.01, (○) 0.2.

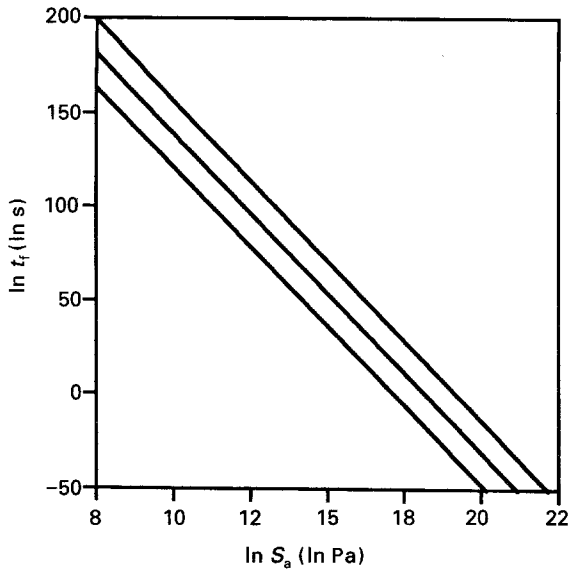

Figure 4 Time-to-failure diagram for Li_2O–Al_2O_3–SiO_2 glass-ceramic from dynamic fatigue data; F = 0.001 with 90% confidence limits.

a function of stressing rate, σ. The dependence of median strength on stress rate indicates that subcritical crack growth is taking place prior to failure. Similar data were presented for the previous study [2].

A linear regression analysis of ln S_f on ln σ yields estimates of the slope and intercept from which the fatigue constants N and B are calculated. The values of N and B were found to be 17 and 1.72×10^{15} $Pa^2 s^{-1}$, respectively. These two values, together with the inert Weibull modulus and the inert Weibull scaling factor were used to construct the time-to-failure diagram shown in Fig. 3, utilizing Equation 1. The diagram was constructed for the probabilities of failure, 0.001, 0.01, and 0.2. Owing to the uncertainty in estimates of N, B, m, and S_o, large uncertainties in calculated lifetimes may occur. For example, in the present study the variances in N and ln B were found

TABLE II Comparison of fatigue parameters of 230/270 grit and polished Li_2O–Al_2O_3–SiO_2 glass-ceramic

Constants	230/270	Polished
N	20	17
B	7×10^{12}	1.7×10^{15}
$V(\ln S_i)$	2.7	1.08
$V(N)$	1.3	0.313

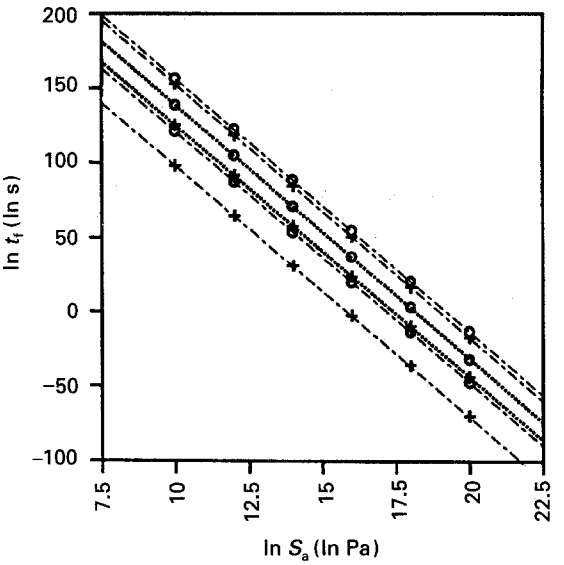

Figure 5 Comparison of time-to-failure (TTF) curves for 230/270 surface determined with fatigue constants from polished and 230/270 grit samples and inert strength data from 230/270 grit samples.

to be 1.08 and 0.313, respectively. The values were determined from equations derived in [16]. Therefore, confidence intervals were calculated using a statistical analysis based on the theory of error propagation [17]. In this instance, the error analysis developed by Ritter *et al.* was used to calculate 90% confidence intervals for the 0.001 failure probability curve, Fig. 4.

The effects of residual stress on lifetime can be seen when comparing the results of this study with those of the previous study, Table II. The derivation of the dynamic fatigue equations is based on the critical stress-intensity factor for Mode I failure, $K_{IC} = Y\sigma_c a_c^{1/2}$, and the power-law relation for subcritical crack-growth velocity to critical size, $V = AK_I^N$. It has been shown that the stress-intensity factor, K, in the presence of residual stress is the sum of two terms: a residual stress term, K_r, and an applied stress term, K_a [11, 12]. The inability to represent K_r in the dynamic fatigue equations for machined flaws prevents the accurate assessment of its influence on time-to-failure. This influence can be seen in the fatigue parameters, N and B, of these two studies, Table II.

The question in design applications is which fatigue parameters are the best to use? Fig. 5 shows the time-to-failure curves for 0.001 probability of failure using both sets of fatigue parameters, and the inert Weibull parameters for the 230/270 grit surface. This demonstrates that using the fatigue parameters determined with the 230/270 grit surface are not significantly

different from those with the polished surface. Although the lower bound of the polished samples is more conservative, neither time-to-failure curves lies beyond the upper or lower bound of the confidence limits. Therefore, designers preferring conservative limits should use samples without residual stress present to determine the fatigue parameters and inert Weibull parameters from samples with the service condition surface, to determine the time-to-failure of the part.

Acknowledgements

The authors thank Ed Horton, Charile Griffth, Tom Kester, and Raj Khanijow for sample preparation.

References

1. H. SCHEIDLER and E. RODEK, *Am. Soc. Bull.* **68** (1989) 1926.
2. D. S. TUCKER *J. Am. Ceram. Soc.* **73** (1990) 2528.
3. J. E. RITTER and J. A. MEISEL *ibid.* **59** (1976) 478.
4. A. G. EVANS and H. JOHNSON, *J. Mater. Sci.* **2** (1976) 214.
5. J. E. RITTER, in "Fracture Mechanics of Ceramics", edited by R. C. Bradt, D. P. H. Hasselman, and F. F. Lange (Plenum Press, New York, 1978) pp. 667–86.
6. H. C. CHANDAN, R. C. BRADT, and G. E. RINDONE, *J. Am. Ceram. Soc.* **61** (1978) 207.
7. K. JAKUS, D. C. COYNE, and J. E. RITTER, *J. Mater. Sci.* **10** (1978) 2071.
8. S. M. WIEDERHORN, A. G. EVANS, E. R. FULLER and H. JOHNSON, *J. Am. Ceram. Soc.* **57** (1974) 319.
9. K. K. SMYTH and M. B. MAGIDA, *J. Am. Ceram. Soc.* **66** (1982) 500.
10. S. W. FREIMAN, A. C. GONZALEZ, and S. M. WEIDERHORN, *Am. Ceram. Soc. Bull.* **63** (1984) 597.
11. D. B. MARSHALL and B. R. LAWN, *J. Am. Ceram. Soc.* **63** (1980) 532.
12. D. B. MARSHALL and B. R. LAWN, *Commun. J. Am. Ceram. Soc.* **64** (1981) C-6.
13. D. B. MARSHALL and B. R. LAWN, in "Fracture in Ceramic Materials", edited by A. G. Evans (Noyes, Park Ridge, NJ 1984) p. 222.
14. E. Y. ROBINSON, "Estimating Weibull Parameters for Materials", NASA Report no. TM 33-580, Jet Propulsion Laboratory, Pasadena, CA (1972).
15. Standard DIN 52 292, Part 1, Testing of Glass and Glass-Ceramics; Determination of Bending Strength, Double-Ring Bending Test on Flat Plate Specimens with Small Test Areas" (1984).
16. J. E. RITTER, N. BANDYOPADHYAY, and K. JANUS, *Am. Ceram. Soc. Bull.* **60** (1981) 798.
17. P. R. BEVINGTON "Data Analysis and Error Reduction in the Physical Sciences" (McGraw-Hill, New York, 1969) pp. 56–64.

Received 1 September 1993
and accepted 8 September 1994